LUND UNIVERSITY

Collective vibrational states within the fast iterative quasiparticle random-phase approximation method

Carlsson, Gillis; Toivanen, J.; Pastore, A.

Link to publication

Total number of authors:
3

Collective vibrational states within the fast iterative quasiparticle random-phase approximation method

B. G. Carlsson,[1,*] J. Toivanen,[2] and A. Pastore[3]

[1]*Division of Mathematical Physics, LTH, Lund University, Post Office Box 118, S-22100 Lund, Sweden*
[2]*Department of Physics, University of Jyväskylä, Post Office Box 35 (YFL) FI-40014, Finland*
[3]*Université de Lyon, Université Lyon 1, CNRS/IN2P3 Institut de Physique Nucléaire de Lyon, F-69622 Villeurbanne cedex, France*

An iterative method we previously proposed to compute nuclear strength functions [Toivanen *et al.*, Phys. Rev. C **81**, 034312 (2010)] is developed to allow it to accurately calculate properties of individual nuclear states. The approach is based on the quasiparticle random-phase approximation (QRPA) and uses an iterative non-Hermitian Arnoldi diagonalization method where the QRPA matrix does not have to be explicitly calculated and stored. The method gives substantial advantages over conventional QRPA calculations with regards to the computational cost. The method is used to calculate excitation energies and decay rates of the lowest-lying 2^+ and 3^- states in Pb, Sn, Ni, and Ca isotopes using three different Skyrme interactions and a separable Gaussian pairing force.

PACS number(s): 21.60.Jz, 21.10.Re

I. INTRODUCTION

The goal of nuclear structure theory is to be able to predict and model the physics of the atomic nucleus. This involves the ground-state properties, as well as different modes of excitation and decay. One of the possible methods to compute excited states in nuclei is based on the quasiparticle random-phase approximation (QRPA) [1]. This approach can be derived by considering the linear response of a nucleus when perturbed by an external field. From the response one can extract information about excited nuclear states and cross sections for nuclear reactions. The QRPA approach is particularly interesting in connection with nuclear density-functional theory (DFT), as the method can be applied also when starting from a density functional. In order for the QRPA method to be practical, it is very important to implement it in ways that have low computational costs. For phenomenological DFT approaches, a low computational cost would allow dynamical properties to be considered when fine tuning model parameters. A numerically efficient method is also essential for applications to deformed and heavy nuclei which are otherwise prohibited by the time and memory required to construct and diagonalize the large QRPA matrix.

Two recent solution methods address these issues. The finite amplitude method (FAM) [2,3] generates the response of a nucleus to an external field by solving the linear response equations iteratively for each requested external field frequency. FAM furthermore uses the same mean fields as in the Hartree-Fock-Bogoliubov (HFB) ground-state calculation and employs finite differences to linearize the equations of motion. In its current form, FAM uses a smoothing method to improve stability and therefore one cannot easily extract the exact QRPA eigenamplitudes. The same is true for the iterative Arnoldi method [4], which is able to provide smoothened QRPA strength functions and their energy weighted moments, but does not generate accurate individual states. A common

aspect of both methods is, however, their ability to generate partial solutions of the full QRPA problem with reduced computational effort. It should be mentioned that both these methods use the full residual interaction when solving the QRPA equations. This distinguishes the approaches from alternative ways to simplify the QRPA problem by constructing separable approximations for the residual interaction [5].

The purpose of this paper is to generalize the Arnoldi method which we previously developed for iterative calculations of RPA strength functions. The generalization involves modifying the method so that it becomes possible to not only compute strength functions but also sets of individual excited states with high accuracy. As a first step the new method is applied to the calculation of excitation energies and decay rates of the lowest lying 2^+ and 3^- states in several isotope and one isotone chain. Particular focus is given to the region around double-magic ^{208}Pb, where new experiments are currently planned [6].

This paper is organized as follows: in Sec. II the QRPA formalism is briefly reviewed and specific aspects of our formulation are discussed. In Sec. III the computational cost and accuracy of the method is evaluated. In Sec. IV the method is applied to the calculation of energies and transition probabilities of the lowest $J^\pi = 2^+$ and $J^\pi = 3^-$ states in a selection of semimagic even-even nuclei. Finally conclusions are given in Sec. V.

II. QRPA IN TERMS OF FIELDS

The iterative method is based on the QRPA equations [1,7–9] which can be derived by starting from time-dependent HFB theory. Here we present the main parts of the derivation, highlighting aspects relevant to the iterative formulation. In cases where the expressions are not fully defined we use notation consistent with Ref. [1].

The QRPA equations can be derived by considering a general time-dependent wave function which is oscillating between the ground state and an excited state with excitation

*gillis.carlsson@matfys.lth.se

energy $\hbar\omega$,

$$|\psi(t)\rangle = e^{-itE_{gs}/\hbar}C_{gs}|\psi_{gs}\rangle + e^{-it(E_{gs}+\hbar\omega)/\hbar}C_{exc}|\psi_{exc}\rangle.$$

We limit the consideration to small-amplitude oscillations around the ground state so that the corresponding generalized density matrix $\mathcal{R}$ [1] can be expanded to first order in C_{exc},

$$\mathcal{R}(t) \simeq \mathcal{R}_{gs} + e^{-i\omega t}\tilde{\mathcal{R}} + e^{i\omega t}\tilde{\mathcal{R}}^{\dagger}.$$

In order to make use of the time-dependent Hartree-Fock-Bogoliubov (TDHFB) equations of motion, it is desired that the time-dependent density should be a HFB density at all times (i.e., it should be a projector $\mathcal{R}^2 = \mathcal{R}$). We further assume that $\mathcal{R}_{gs}$ can be approximated with the ground-state HFB density. Then the most general approximation for the transition density which ensures that $\mathcal{R}(t)$ is a projector during small-amplitude vibrations involves both the forward $\tilde{Z}$ and the backward $\tilde{Z}'^{\dagger}$ going amplitudes,

$$\mathcal{U}^{\dagger}\tilde{\mathcal{R}}\mathcal{U} = -C_{gs}^{*}C_{exc}\langle\psi_{gs}|\begin{pmatrix} \alpha\alpha^{\dagger} & \alpha\alpha \\ \alpha^{\dagger}\alpha^{\dagger} & \alpha^{\dagger}\alpha \end{pmatrix}|\psi_{exc}\rangle$$
$$\simeq \begin{pmatrix} 0 & \tilde{Z} \\ \tilde{Z}'^{\dagger} & 0 \end{pmatrix}. \quad (1)$$

In this expression we have made use of the matrix

$$\mathcal{U} = \begin{pmatrix} U & V^{*} \\ V & U^{*} \end{pmatrix},$$

written in terms of the U and V pairing matrices [1] related to the HFB ground state as well as the matrices of quasiparticle operators $[\alpha\alpha^{\dagger}]_{ij} = \alpha_i\alpha_j^{\dagger}$. It should be noted that if the wave functions in the beginning were taken as HFB vacuums one would not obtain any backward going amplitudes, as can be seen from Eq. (1) by inserting the HFB ground state. Thus it is the assumption of the transition density $\tilde{\mathcal{R}}$ being as general as allowed by the $\mathcal{R}^2 = \mathcal{R}$ criteria which allows for the existence of the implicitly defined correlated ground state.

Inserting the expression for $\mathcal{R}(t)$ into the TDHFB equations of motion $i\hbar\frac{d\mathcal{R}(t)}{dt} = [\mathcal{H}, \mathcal{R}(t)]$ [9] and taking the small-amplitude limit leads to the QRPA equation

$$\hbar\omega\tilde{\mathcal{R}} \simeq [\mathcal{H}[\mathcal{R}_{gs}], \tilde{\mathcal{R}}] + [\mathcal{H}^1[\tilde{\mathcal{R}}], \mathcal{R}_{gs}].$$

In this expression the hermicity property $\mathcal{H}^1[\tilde{\mathcal{R}}] = (\mathcal{H}^1[\tilde{\mathcal{R}}^{\dagger}])^{\dagger}$ of the effective interaction was assumed and the time-dependent fields $\mathcal{H}(t) = \partial\mathcal{E}/\partial\mathcal{R}$ were expanded around the ground-state value

$$\mathcal{H}[\mathcal{R}] \simeq \mathcal{H}[\mathcal{R}_{gs}] + \mathcal{H}^1[\mathcal{R} - \mathcal{R}_{gs}].$$

This expansion is taken to first order in the transitional fields, which is enough for small-amplitude vibrations and leads to

$$\mathcal{H}^1[\tilde{\mathcal{R}}] = \begin{pmatrix} \tilde{h} & \tilde{\Delta} \\ \tilde{\Delta}'^{\dagger} & -\tilde{h}^T \end{pmatrix},$$

where

$$\tilde{h}_{\mu\nu} = \sum_{\pi\lambda}\left.\frac{\partial h_{\mu\nu}}{\partial\rho_{\pi\lambda}}\right|_{\rho_{gs}}\tilde{\rho}_{\pi\lambda},$$

$$\tilde{\Delta}_{\mu\nu} = \frac{1}{2}\sum_{kl}v^{pp}_{\mu\nu kl}\tilde{\kappa}_{kl},$$

$$\tilde{\Delta}'^{*}_{\mu\nu} = \frac{1}{2}\sum_{kl}v^{pp*}_{\mu\nu kl}\tilde{\kappa}^{*}_{kl}.$$

In our case with a density-independent pairing interaction it is only the $h = \partial\mathcal{E}/\partial\rho$ field which is nonlinear in the densities and becomes linearized. With a density-dependent pairing interaction the $\tilde{\Delta}, \tilde{\Delta}'$ fields would also have to be linearized and would give an additional contribution to the $\tilde{h}$ field.

Inserting the expressions for fields and densities into the QRPA equation, and multiplying from the left with $\mathcal{U}^{\dagger}$ and from the right with $\mathcal{U}$, gives a system of equations for the unknown excitation energies $\hbar\omega$ and the $\tilde{Z}$ and $\tilde{Z}'$ amplitudes:

$$\hbar\omega\tilde{Z} = E\tilde{Z} + \tilde{Z}E + \tilde{W},$$
$$-\hbar\omega\tilde{Z}'^{\dagger} = E\tilde{Z}'^{\dagger} + \tilde{Z}'^{\dagger}E + \tilde{W}'^{\dagger}.$$

In this equation, E denotes a diagonal matrix of positive quasi-particle energies and the $\tilde{W}$ matrices depend on the linearized fields

$$\tilde{W} = U^{\dagger}\tilde{h}V^{*} + U^{\dagger}\tilde{\Delta}U^{*} + V^{\dagger}\tilde{\Delta}'^{\dagger}V^{*} - V^{\dagger}\tilde{h}^TU^{*},$$
$$\tilde{W}'^{\dagger} = V^T\tilde{h}U + V^T\tilde{\Delta}V + U^T\tilde{\Delta}'^{\dagger}U - U^T\tilde{h}^TV, \quad (2)$$

which can be expressed in terms of the transition densities

$$\tilde{\rho} = U\tilde{Z}V^T + V^*\tilde{Z}'^{\dagger}U^{\dagger},$$
$$\tilde{\kappa} = U\tilde{Z}U^T + V^*\tilde{Z}'^{\dagger}V^{\dagger}, \quad (3)$$
$$\tilde{\kappa}'^{\dagger} = V\tilde{Z}V^T + U^*\tilde{Z}'^{\dagger}U^{\dagger}.$$

It is instructive to look back and consider the approximations used in the derivation of these equations. The main approximations appear to be the use of the TDHFB equations of motion, which restricts us to the consideration of excited states connected by two quasiparticle operators to the ground state and the assumption that the ground-state density can be approximated with the density of the HFB ground state.

As an example to illustrate the iteration procedure, we neglect spin and isospin and consider a term in the energy of the form

$$\mathcal{E}[\rho] = \int\rho^{\alpha+2}(\vec{r})d\vec{r},$$

which gives the linearized field

$$\tilde{h}_{im} = (\alpha+2)(\alpha+1)\int\phi_i^{*}(\vec{r})\big(\rho^{\alpha}_{gs}(\vec{r})\tilde{\rho}(\vec{r})\big)\phi_m(\vec{r})d\vec{r}.$$

In this case, the action of the QRPA matrix on an eigenvector can be calculated in three steps.

The first step is to generate the densities $\tilde{\rho}$ according to Eq. (3) and to express them in r space. For the next step, $\tilde{h}$ is calculated as above. Alternatively, in the case of a density-independent interaction, where fields are already linear in densities $\mathcal{H}^1[\tilde{\mathcal{R}}] = \mathcal{H}[\tilde{\mathcal{R}}]$, this can be achieved using the HFB mean-field routines for calculating matrix elements.

Finally multiplying the fields with U and V matrices as in Eq. (2) one obtains the W matrices.

The main advantage of expressing the equations in this form is that calculating and storing two-body matrix elements can be avoided and instead one can rely on the expressions for HFB fields. The price to pay is that the densities and integrals for the matrix elements of the fields are recalculated for each matrix vector product, in the same way as when performing the HFB iterations to find the ground state. Thus it is important to investigate how many iterations, i.e., matrix-vector products are needed in order to obtain acceptable convergence, and whether the iteration procedure introduces numerical errors which could lead to instabilities.

III. ACCURACY AND EFFICIENCY OF THE METHOD

The iterative QRPA solver is implemented by extending the program HOSPHE (v1.02) [10] and will be included in the next published version of the program. This code uses a spherical harmonic oscillator basis and takes advantage of the Wigner-Eckart theorem in order to work with angular momentum reduced quantities. The use of reduced quantities keeps the HFB and QRPA dimensions small and makes the code a useful tool for testing different calculational methods.

In order to verify that the QRPA implementation is correct, a comparison is made with a recent QRPA implementation based on the HFBTHO code [11]. This code is able to treat axially deformed nuclei and its QRPA implementation is based on the traditional diagonalization of a large QRPA matrix. Therefore, applications of this code are limited to cases where dimensions can be kept within manageable limits.

As a test case we consider the nucleus $^{18}_{8}O_{10}$ and compare the ground-state energy and energies of the QRPA excitations obtained in both codes. In order to have a benchmark result that is useful for testing future QRPA codes we list values obtained from both codes in Table I. Several different recipes on how to truncate the pairing space and how to treat the Coulomb interaction exist in the literature, so in order to make the benchmark results as useful as possible, the results are obtained without any pairing truncation and without any Coulomb interaction. The remaining parameters are listed in the caption of Table I.

The implementation based on the axially deformed HFBTHO code [11] allows us to test its accuracy by performing calculations for excitations with different angular momentum projections on a principal axis of the nucleus. Since the comparison is made for a spherical nucleus, these different calculations should ideally give the same result. In this way, for the QRPA implementation of Ref. [11], the precision of the 2^+ excitation was estimated to be roughly 10^{-4} both for the energy and for the $B(E2)$ value. As seen from Table I, the lowest states calculated with both codes agree to about this precision. A similar accuracy test with the HOSPHE code is not possible as it works in spherical symmetry. But since HOSPHE uses the same mean fields both in the QRPA and the HFB calculations we expect about the same accuracy for the QRPA excitations as for the ground-state energy. The full strength functions calculated with both codes were also compared and

TABLE I. Comparison of HFB and QRPA calculations performed for the nucleus ^{18}O without any pairing truncation and without Coulomb interaction. For the Skyrme interaction we use the SLy4 parametrization [12] with a δ (volume) pairing interaction [13] with strength $V_0 = -200$ MeV (fm)^3 and a one-body center-of-mass correction. The results are obtained with a harmonic oscillator basis where the maximum oscillator shell included has principal quantum number $N_{max} = 5$ and the oscillator constant is set to 0.865 (fm)$^{-1}$. In this table, the transition strengths are calculated using the isoscalar transition operators of Ref. [14]. Energies have units of MeV and the $B(EI)$ values are in units of e^2(fm)$^{2I+4\delta_{I,0}}$. For each multipolarity the state lowest in energy with an appreciable strength is compared. When both codes give the same decimals, they are printed in bold.

Quantity	HOSPHE	HFBTHO + QRPA [11]
E_{HFB}	**−131.6770225**32	**−131.6770225**19
$E(0^+)$	**20.49599**056	**20.49599**7
$E(1^-)$	**14.020**98740	**14.020**85
$E(2^+)$	**8.69120**0427	**8.69120**
$E(3^-)$	**12.91748**593	**12.91747**
$E(4^+)$	**9.041422**878	**9.041425**
$B(E0: 0^+ \rightarrow 0^+)$	**0.020567**096	**0.0205675**
$B(E1: 0^+ \rightarrow 1^-)$	**12.8061**5358	**12.8058**
$B(E2: 0^+ \rightarrow 2^+)$	**0.3352**04540	**0.3352**

turned out to be indistinguishable by eye when the reduced transition probabilities are plotted as function of the energy of the excited states.

A. Iterative solutions

As described above, the product of the QRPA matrix acting on an arbitrary vector can be calculated without constructing the matrix explicitly. When this technique is used, traditional matrix diagonalization routines, which need explicit information about the matrix elements, cannot be used. Instead, one must resort to indirect iterative methods, such as the Lanczos or Arnoldi [15] methods. For non-Hermitian problems, such as the QRPA eigenvalue problem, the implicitly restarted Arnoldi (IRA) method [16,17] is one of the most commonly used methods for finding accurate approximations for the eigenstates lowest in energy. The IRA method is a more advanced version of the original Arnoldi method, giving faster convergence and a reduction in computational effort. As with the iterative Arnoldi method of Ref. [4], the IRA method generates a set of basis vectors, usually called Ritz vectors, which span a vector space called the Krylov subspace, and uses these vectors to represent the QRPA eigenvectors. However, the IRA method's use of restarting allows it to gradually improve the accuracy of a set of eigenstates during iteration, using a reasonably small number of Ritz vectors (typically a few hundred at most).

In the extended HOSPHE code, we use the numerical software ARPACK [18], which implements the IRA method. With this method, the number of matrix-vector products needed in order to reach convergence depends on the requested tolerance. Denoting the QRPA matrix A, the approximate eigenvector x, and the corresponding approximate eigenvalue λ, the iterations
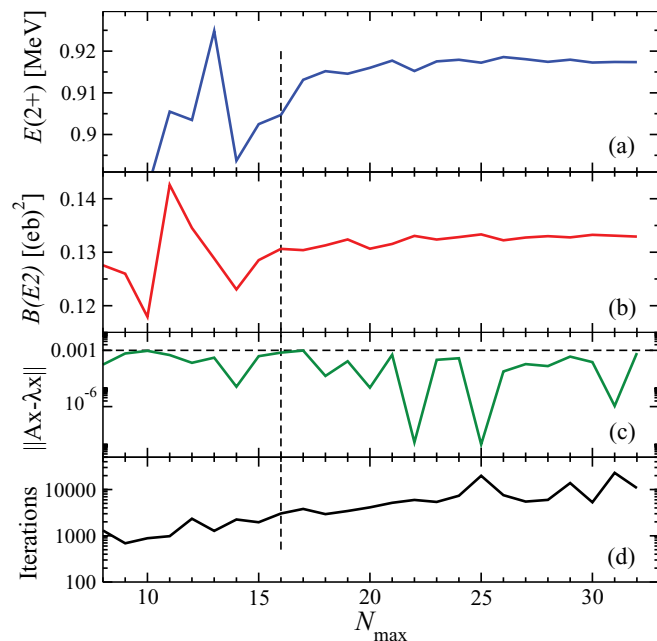
FIG. 1. (Color online) Convergence of excitation energy and reduced transition probability are shown in panels (a) and (b) for the lowest 2^+ state in ^{214}Pb using the SLy4 interaction together with a separable Gaussian pairing force [19–23]. The convergence is shown as a function of the maximum oscillator shell N_{max} included in the basis. The accuracy measure and the number of iterations needed to obtain convergence are shown in panels (c) and (d) respectively. The tolerance parameter which determines when to stop the Arnoldi iterations was set to 0.001. For $N_{max} = 16$, the wall-clock time was 12 min on a desktop workstation (Intel Core i7-2600K, 3.4 GHz). In all cases the Krylov subspace was constructed from 100 Ritz vectors which was estimated to give the fastest convergence with $N_{max} = 16$.

proceed until the accuracy measure $\|Ax - \lambda x\|$ [18] is less than the requested tolerance.

Figure 1 shows the convergence as a function of the basis size when applying the method for the calculation of the lowest 2^+ state in ^{214}Pb. The only truncation employed is the number of main oscillator shells used for the basis. As seen from this figure the accuracy measure is always lower than the requested tolerance when the iterations finish, and the number of iterations required in order to reach the desired convergence increases with the size of the basis.

To find the lowest eigenstates a typical choice is to start from a random initial guess (pivot) vector. For states with large transition probabilities, the number of iterations needed can however be reduced by instead starting from an initial pivot vector whose matrix elements are set to the matrix elements of the corresponding electromagnetic multipole operator [4]. In the case where pairing disappears (and the numerical accuracy is high) the electromagnetic pivot also filters out the states that have an overlap with the pivot and thus removes states which correspond to pair addition or removal. Because of these advantageous features we start from an electromagnetic pivot in all the calculations presented.

For the calculations presented below, a value of 17 oscillator shells ($N_{max} = 16$) was chosen to offer a good balance

between accuracy and computational speed. Assuming that the calculation with 33 oscillator shells shown in Fig. 1 is fully converged, the truncation error when stopping at 17 shells amounts to 0.01 MeV for the energy and 0.002 $(e b)^2$ for the reduced transition probability. Using 17 shells reduces the dimension of the QRPA matrix to 8016 as compared to 59296 in the case of 33 shells. With this smaller basis and using a tolerance parameter of 0.001, the average time to calculate the lowest state for a nucleus in the lead isotope chain is 6.5 min (Intel Core i7-2600K, 3.4 GHz) and the average number of iterations required is 2663.

Sets of a few lowest eigenvalues can also be extracted and require about the same number of iterations. For example, in the case of ^{192}Pb, the number of iterations needed to extract 10, 20, and 30 positive energy eigenstates becomes 1974, 2648, and 3427 respectively.

IV. NUMERICAL RESULTS

A. Influence of the pairing interaction

In order to study the influence of the pairing interaction on 2^+ states we compare the use of a zero-range δ interaction [13] combined with a truncation in the equivalent spectra [24] to the use of a separable Gaussian pairing force [19–23]. This force has a finite range and therefore does not need to be truncated. In order to obtain reasonable pairing, the pairing strengths are tuned to get the lowest quasiparticle energies to agree with the experimental gaps extracted in Ref. [25] using a four-point formula. The resulting parameters obtained for the finite-range interaction are shown in Table II.

Results for the lead isotopes using the different pairing interactions are shown in Fig. 2. As seen in this figure there are fluctuations in the energies which depend on the choice of pairing force. Comparing the two pairing interactions, it appears that the finite-range interaction is slightly better in capturing the fluctuations of the experimental energies.

In the equivalent spectra method the normal and abnormal density-matrices are truncated during the HFB iterations [24]. However, in the subsequent QRPA calculation we used nontruncated wave functions without any energy cut for the residual particle-particle interaction. This way of using the equivalent spectra method is therefore slightly inconsistent, and a better truncation recipe is desired. In the following we will only use the finite-range pairing interaction which does not need to be truncated and allows us to treat HFB and QRPA in a consistent way.

The effect of changing the strength of the Gaussian pairing interaction with $\pm 5\%$ is shown in Fig. 2 with dashed lines.

TABLE II. Strength parameters of the separable Gaussian pairing interaction in units of MeV fm^3. For the range of the interaction we adopt the value $a = 0.660$ fm in all cases.

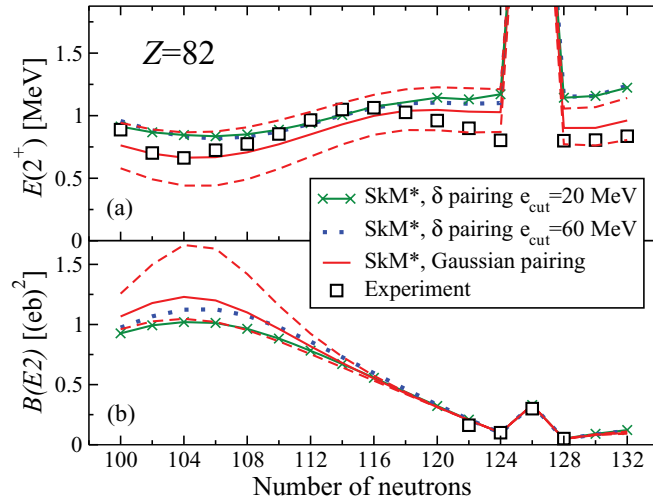| Interaction	G_n	G_p
SLy4	655	600
SKM*	610	550
SkX	560	530

FIG. 2. (Color online) Panel (a) shows excitation energies and panel (b) reduced transition probabilities [$B(E2; 0_{gs}^+ \rightarrow 2_1^+)$] for Pb isotopes. Results are shown for different treatments of the pairing interaction. The dashed lines denote the result of changing the strength of the finite-range pairing with $\pm 5\%$. Decreasing the pairing lowers the energies and raises the $B(E2)$ values. The strength parameters for the zero-range interaction were chosen as $V_n = -168$ and $V_n = -200$ MeV (fm)^3 when the cutoff in the equivalent spectra was taken as 60 and 20 MeV respectively.

Both the energies and the transitions are sensitive to such a change, i.e., a decrease of the pairing lowers the excitation energies and raises the $B(E2)$ values. The effect is seen to be largest for $N = 104$ which is just between two magic numbers. The schematic fits of the pairing strengths appear to give quite reasonable values for the lead isotopes with an average $E(2^+)$ energy that agrees roughly with experiment.

B. $J^\pi = 2^+$ states in Pb and Sn isotopes

In this work we consider three different Skyrme parametrizations: SkM*, SLy4, and SkX. SKM* is based on the SkM parameters [26], but has been adjusted further using results from fission barrier calculations [27]. The original SkM parameters were determined by considering both static ground-state properties as well as some dynamical properties including monopole and quadrupole resonances [26]. SLy4 was adjusted with special care taken to model neutron matter in order to facilitate the description of neutron-rich nuclei [12]. The accuracy of QRPA based on these interactions was recently studied and compared to calculations based on the generator-coordinate method GCM [28]. It was found that SkM* reproduced experimental 2^+ states more accurately than SLy4 and the QRPA results were similar to results obtained with the GCM. In addition, we also consider the SkX interaction which has been tuned with special focus on reproducing single-particle states in double-magic nuclei [29].

Results for the lead isotopes using the three different Skyrme interactions are shown in the left hand panels of Fig. 3.

For the double-magic nucleus Pb$_{126}$, SkX gives the correct 2^+ energy while the other two forces overestimate this
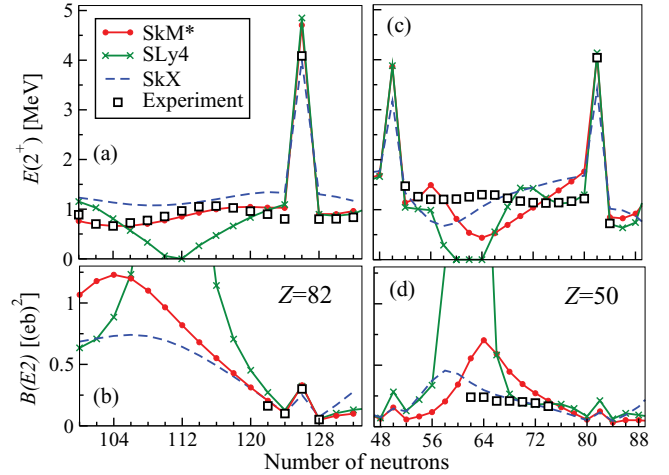

FIG. 3. (Color online) Excitation energies and reduced transition probabilities [$B(E2; 0_{gs}^+ \rightarrow 2_1^+)$] for Pb and Sn isotopes. Results are shown for three different Skyrme parametrizations. The experimental values are taken from Ref. [30].

excitation energy. As the neutron number is reduced, the predictions show considerable differences. SLy4 gives zero-energy solutions around $N = 112$, indicating a transition to a deformed ground state, while the other two interactions appear to be stiffer towards deformation and give more realistic results.

The ground-state energies of Pb$_{108}$ and Pb$_{112}$ as a function of quadrupole deformation are shown in Fig. 4. The energy curves are calculated using δ pairing instead of the Gaussian pairing which means that the curves are slightly inconsistent with the QRPA calculations, but the general features will be
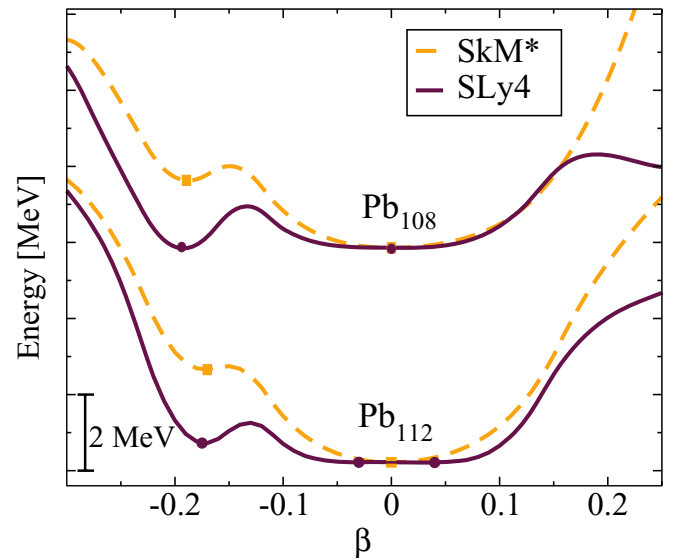

FIG. 4. (Color online) HFB ground-state energy as a function of quadrupole deformation β [24] for Pb$_{108}$ and Pb$_{112}$. The calculation was performed using the HFBTHO code [24]. The local minimas are marked with symbols. Constant shifts of both curves have been applied in order to make them fit in the figure.

the same. As seen from this figure, both interactions predict spherical minima for Pb$_{108}$, although the lowest minimum with SLy4 is the oblate one with quadrupole deformation $\beta = -0.19$. The spherical minimum obtained with SkM* is stiffer than with SLy4 which is probably the reason why the 2^+ energy is predicted higher. As one moves to Pb$_{112}$, SLy4 gives the spherical point as a maximum with neighboring slightly deformed minima. In this case our QRPA calculation is likely to give a zero-energy solution as the assumed spherical ground state is no longer stable with respect to quadrupole deformations. The 2^+ energies obtained with the SkM* interaction agree rather well with experiment and seem to favor the prediction of stiffer energy surfaces.

Because of shape coexistence, especially the lighter lead isotopes ($N = 100$–106) are expected to have competing 2^+ states resulting from excitations in different minima. The nature of the lowest 2^+ state in Pb$_{106}$ was investigated using a band-mixing calculation in Ref. [31]. The results from this calculation are that the ground state is estimated as 95% "spherical" and the first 2^+ state as 18% "spherical" and 69% "prolate". In this work we blindly compare the lowest calculated excitations based on the spherical minimum with the lowest experimental excitations, and a full investigation of the competition between excitations in different minima will have to wait for a deformed version of our method.

In the QRPA formalism, an expression for the operator which creates the excited states by acting on the QRPA ground state can be written as

$$O_\alpha^\dagger = \sum_{k<k'} Z_{kk'}^\alpha \alpha_k^\dagger \alpha_{k'}^\dagger - Z_{kk'}^{\prime\alpha*} \alpha_{k'} \alpha_k.$$

In order to discuss the structure of the solutions, we label the kk' components of this creation operator using the quantum numbers of the quasiparticle operators. As an example, if both k and k' refer to a quasiproton (quasineutron) in a $i_{13/2}$ shell, the corresponding component is denoted as $\pi(i_{13/2})^2$ ($\nu(i_{13/2})^2$). Indeed, in the limit when $Z_{kk'}^{\prime\alpha} = 0$ this turns into the usual notation for writing two quasiprotons (quasineutrons) in the $i_{13/2}$ shell.

The major oscillator N_{osc} quantum number is not preserved in the calculations, but for simplicity we will refer to the mixed orbitals using the harmonic oscillator ordering. For example the lowest $p_{3/2}$ and $p_{1/2}$ quasiparticle orbitals will be referred to as being of $N_{osc} = 1$ character, although these orbitals also contain contributions from higher oscillator shells.

We denote the probability $P_{\alpha j,\alpha' j'}$ for different components in the wave functions of the excited states by summing contributions from the different m quantum numbers as

$$P_{\alpha j,\alpha' j'} = \sum_{m,m'} |Z_{\alpha jm,\alpha' j'm'}|^2 - |Z_{\alpha jm,\alpha' j'm'}'|^2.$$

Defined in this way, the largest components in the calculated 2_1^+ states in the chain of lead isotopes are shown in Fig. 5. As seen in this figure, the largest proton and neutron components in Pb$_{126}$ involve particle-hole excitations across the $Z = 82$ and $N = 126$ gaps. In the other isotopes, where neutron pairing is active, the 2^+ states mainly involve neutron excitations ($\sim$85%) with the dominating component being 15%–30% $\nu(i_{13/2})^2$ for $N = 100$–116. The calculated neutron single-
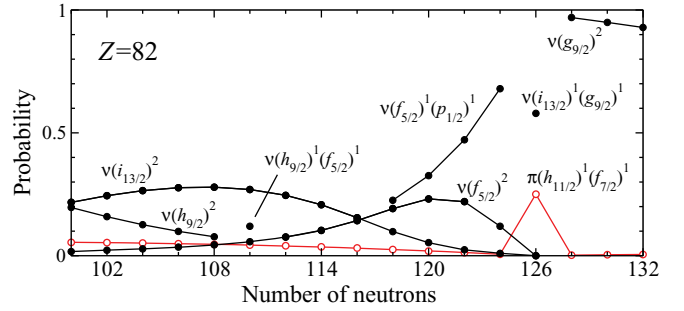

FIG. 5. (Color online) Structure of QRPA 2_1^+ states in lead isotopes using SkM*.

particle levels are shown in Fig. 6, and as expected the dominating components in the 2^+ states involve excitations among the shells close to the Fermi level.

It should be noted that the transition strengths are calculated directly from the electromagnetic operators [1] without any effective charges. Therefore it is the smaller proton components, suppressed because of the magic proton number, which determine the electromagnetic properties. It is also interesting to notice that, above the 126 gap, the 2_1^+ states are composed of rather pure two-quasineutron excitations to the $g_{9/2}$ shell.

For the $N = 126$ isotones shown in Fig. 7 there is a similar accuracy as obtained for the lead isotopes. To have a better idea about the amount of collectivity that should be present when going away from $_{82}$Pb$_{126}$, more experimental transition probabilities are clearly needed and experiments to measure the unknown $B(E2)$ values for the isotopes $_{82}$Pb$_{114,116,118,120}$, $_{78}$Pt$_{122,124}$ and $_{80}$Hg$_{126}$ are planned [6].
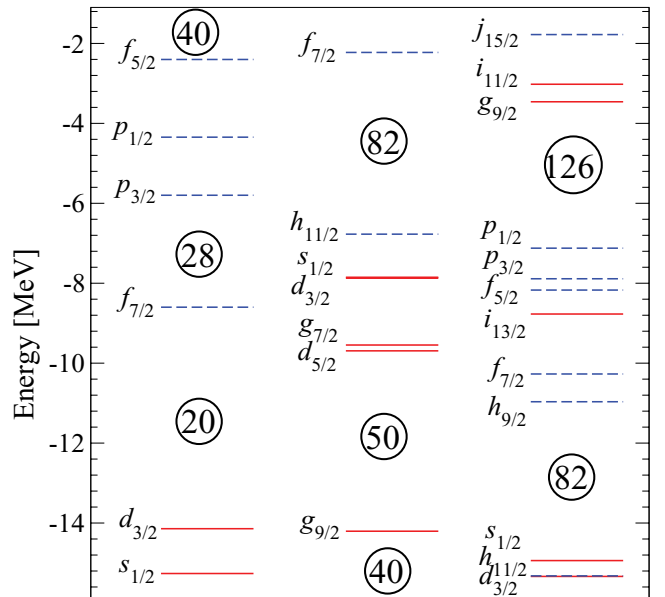

FIG. 6. (Color online) Theoretical (SkX) neutron single-particle levels. The left set of levels is for Ca$_{28}$, the middle set for Sn$_{82}$, and the right set is for Pb$_{126}$. Positive parity levels are shown with full lines and negative parity levels with dashed lines.
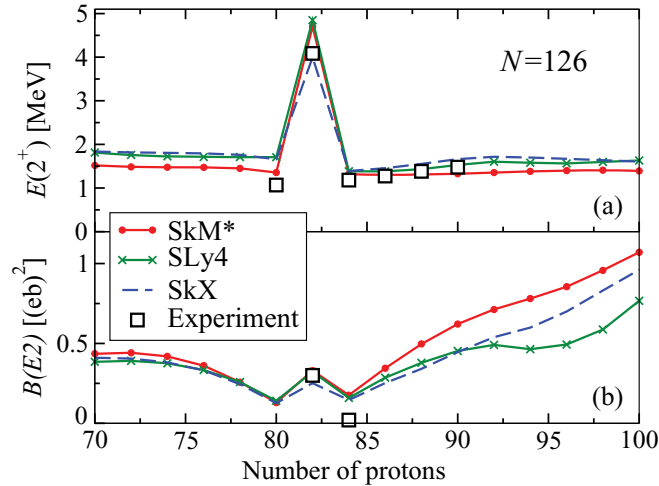
FIG. 7. (Color online) Same as in Fig. 3, but for $N = 126$ isotones.

Results for the Sn chain are shown in the right-hand panels of Fig. 3. As in the case of the Pb chain, the SLy4 interaction gives some zero-energy solutions, while the other two interactions produce dips in the excitation energies for some isotopes, but do not reach zero. For the two double-magic Sn isotopes, the excited states are calculated to be a roughly even mixture of proton and neutron excitations, while the excited states in the semimagic isotopes mainly involve neutron excitations. With SkX, the largest components are $\nu(d_{5/2})^2$ for Sn_{52-54}, $\nu(g_{7/2})^2$ for Sn_{56-64}, and $\nu(h_{11/2})^2$ for Sn_{66-80}. The positions of these shells (shown in Fig. 6) are thus important in order to reproduce the details of the experimental data.

C. $J^\pi = 2^+$ states in Ni and Ca isotopes

The results for the Ni chain are shown in the left-hand panels of Fig. 8. In Ni_{28}, the 2^+ state is built from an almost equal mixture of proton and neutron excitations, while the 2^+ states in the other nickel isotopes are dominated by neutron
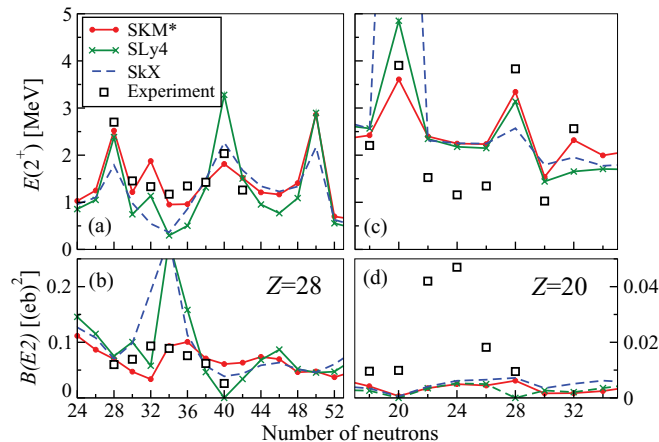

FIG. 8. (Color online) Same as in Fig. 3, but for Ni and Ca isotopes.

excitations. SkX predicts a smaller 28 gap than the other interactions and a 2^+ state in Ni_{28} which is lower than in experiment. SkX also predicts a smaller gap at $N = 32$ and does not show the spike in excitation energy obtained with the other interactions for Ni_{32}.

QRPA calculations based on the relativistic mean-field model for Ni_{40} [32] overpredicted the energy of the 2^+ state by roughly three times the experimental energy. A suggested explanation was missing 2p-2h and higher-order excitations among the neutrons [32]. Since the neutron Fermilevel is located between opposite-parity shells, this state will be overpredicted whenever the neutron pairing goes to zero. With SLy4 we also obtain an overprediction, although less severe, while the other interactions predict excitation energies close to the experimental value. It is interesting to note that with SkX the ground state is calculated to have an average gap [33] of $\Delta_n = 1.38$ MeV and the 2^+ state is obtained with both correct energy and transition strength. The state is built as a mixture of proton ($\sim 23\%$) and neutron ($\sim 77\%$) excitations, where the largest component is $\nu(g_{9/2})^2$.

Results for the Ca chain are shown in the right-hand panels of Fig. 8. For Ca_{20} one should notice that the Fermi levels for both neutrons and protons are right between shells with opposite parity. Therefore, if pairing disappears, as happens with SkX, the lowest particle-hole excitations with positive parity are between shells of $N_{osc} = 2$ and $N_{osc} = 4$ character, and the excitations have to bridge an energy gap of around 15 MeV, which pushes the predicted 2^+ state up to a high energy. With SkM* (SLy4) there is some pairing remaining and a low-lying 2^+ state can be constructed with a dominating $\pi(d_{3/2})^2$ ($\pi(f_{7/2})^2$) quasiparticle component. This state is likely to have an average particle number that is somewhat wrong, but in this work we only remove the excitations being in the wrong nucleus if pairing vanishes completely. Notice also that since the transition operator is of particle-hole type, excitations corresponding to addition or removal of two particles gives zero for the transition strength.

In general, the 2^+ states in the Ca chain are predicted to have too little collectivity compared to experiments. The states in Ca_{22-26} are predicted to be rather pure excitations within the $f_{7/2}$ shell. For example, with the SkX interaction the component of $\nu(f_{7/2})^2$ is 95%, 90%, and 82% for the excitations in Ca_{22-26} respectively. In order to induce more collectivity, it appears likely that proton two-particle–two-hole excitations across the $Z = 20$ gap must be explicitly included, which goes beyond the present QRPA treatment.

D. $J^\pi = 3^-$ states in Pb and Sn isotopes

The calculated 3^- states for lead isotopes are shown in the left-hand panels of Fig. 9. The most striking feature of the data is the dip in excitation energy seen when going from Pb_{126} to Pb_{128}. In Pb_{126} the 3^- state is created by a roughly equal amount of neutron and proton excitations across the 82 and 126 gaps. When two more neutrons are added, negative parity states can be made by exciting particles between the neighboring positive-parity $g_{9/2}$ shell and negative-parity $j_{15/2}$ shell, located above the 126 gap (see Fig. 6). Therefore the 3^-
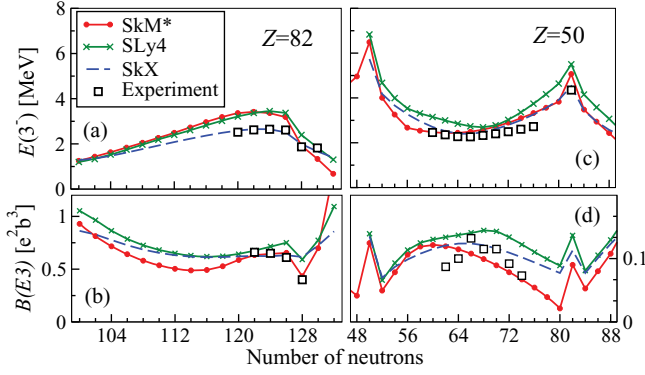
FIG. 9. (Color online) Excitation energies and reduced transition probabilities $[B(E3;0_{gs}^+ \rightarrow 3_1^-)]$ for the lowest 3^- states in Pb and Sn isotopes. Results are shown for three different Skyrme parametrizations. The experimental data for the 3^- states are taken from the compilation in Ref. [34].

FIG. 10. (Color online) Same as in Fig. 9, but for Ni and Ca isotopes.

state in Pb_{128} can be built at a low cost mainly from neutron excitations, which explains the dip in the experimental energy. As seen in Fig. 9, SkX reproduces the experimental lowest 3^- energies and $B(E3)$ values almost perfectly except for the dip in the transition probability seen for Pb_{128}. The forces SkM* and SLy4 have a less perfect overall agreement, but SkM* agrees with experiment in the case of Pb_{128}.

In Pb_{100} with SkX, the excitation operator for the lowest 3^- state consists of 17% proton excitations, where the largest component is only 6% $\pi(d_{3/2})^1(h_{9/2})^1$ and the main neutron component is 62% $\nu(f_{7/2})^1(i_{13/2})^1$. The 3^- states of the neutron-deficient Pb isotopes have many small proton components contributing. When the neutron number increases, proton excitations become more dominant, but with fewer components contributing. At $N = 124$, proton excitations constitute 48% with one dominant component, 29% $\pi(d_{3/2})^1(h_{9/2})^1$, while the largest neutron component is 13% $\nu(p_{3/2})^1(g_{9/2})^1$. Thus, with QRPA, we see a transition from strong proton configuration mixing in Pb_{100} to strong neutron configuration mixing in Pb_{124}.

The lowest experimental and calculated 3^- states of tin isotopes are shown in the right-hand panels of Fig. 9. The energies are reproduced almost perfectly in the region $N = 60$–72, using SkX and SkM* forces. Closer to the $N = 82$ shell closure, the predicted energies become too high. The experimental $B(E3)$ values are reproduced roughly by all three Skyrme forces, but none of the three forces gives a truly accurate description of the finer details. The excitations are dominated by the $\nu(d_{5/2})^1(h_{11/2})^1$ configuration which has a component of 70% in Sn_{52}, and gradually goes down to 50% in Sn_{80}. The second largest excitation is 3% $\nu(g_{9/2})^1(h_{11/2})^1$ in Sn_{52}, but starting from Sn_{54} the second largest excitation is $\nu(g_{7/2})^1(h_{11/2})^1$ and its amplitude grows steadily from 5% to 10% in Sn_{80}. Other neutron excitations between the $\nu h_{11/2}$ subshell and the $N_{osc} = 4$ orbitals are excluded because of angular momentum selection rules. The proton fraction of the transitions is an almost constant 10% and is composed of many small-amplitude excitations. The lowest energies and the largest transitions strengths are obtained for $N = 66$ when
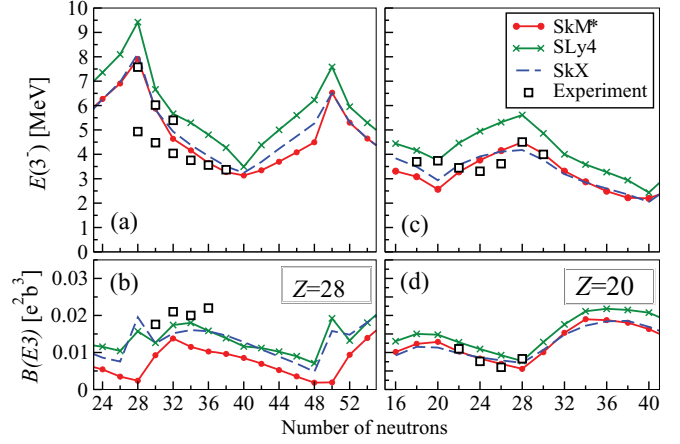
the neutron Fermi level is close to the $\nu h_{11/2}$ intruder shell and negative-parity excitations correspond to a low energy cost.

E. $J^\pi = 3^-$ states in Ni and Ca isotopes

For the Ni isotopes shown in the left hand panels of Fig. 10 we also show experimental data for the second 3^- states in Ni_{28-32} taken from Ref. [35]. For some reason the calculations for Ni_{28-32} agree better with the second 3^- states. Especially the lowest 3^- state in Ni_{28} is predicted about 3 MeV too high in energy. It should be noted that this state has not been clearly identified as 3^- in experiments [34], contrary to the 3^- states in the other Ni isotopes. One should also note that with Skyrme-type interactions one usually neglects proton-neutron pairing and part of the isovector particle-hole interaction which may have an influence around the $N = Z$ line. With SkX, the lowest theoretical 3^- state in Ni_{28} is calculated to be of isoscalar type. This state is built from 28% $\nu(d_{3/2})^1(p_{3/2})^1$ and 22% $\pi(d_{3/2})^1(p_{3/2})^1$ along with smaller probability excitations to the orbitals of $N_{osc} = 4$ character.

For the semimagic nickel isotopes with $N = 30$–48, the 3^- states are dominated by neutron excitations $\nu(p_{3/2})^1(g_{9/2})^1$ which decrease from 75% in $N = 30$ to 16% in $N = 48$, and $\nu(f_{5/2})^1(g_{9/2})^1$ which increase from 2% in $N = 30$ to 74% in $N = 48$. The proton components are small since it is more favorable to excite neutrons when the proton Fermi level is just above $f_{7/2}$. The double-magic Ni_{50} has a different structure than the semimagic isotopes, the dominating component being 36% $\nu(p_{1/2})^1(d_{5/2})^1$.

The results for calcium isotopes are shown in the right-hand panels of Fig. 10. In this case, the lowest experimental 3^- energies are best reproduced by SkM* and SkX while SLy4 gives too high energies. However, in general the finer details of the 3_1^- energies between $N = 20$ and $N = 26$ are not reproduced. Especially for the $N = Z$ nucleus Ca_{20}, the energy calculated with SkM* and SkX becomes too low.

The leading wave-function components of the calcium isotopes are shown in Fig. 11. As seen in this figure, the 3^- state in $_{20}\text{Ca}_{20}$ is composed of a fairly even mixture of proton
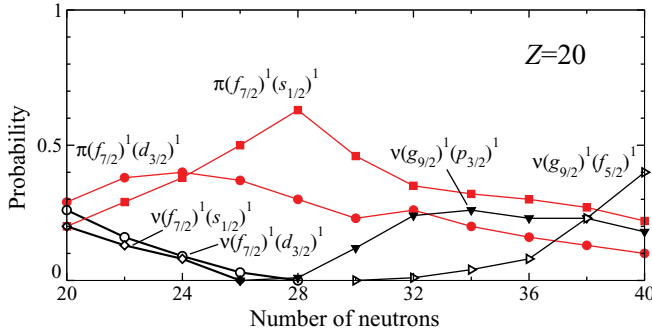
FIG. 11. (Color online) Leading two-quasiparticle components of QRPA 3_1^- states in Ca isotopes using SkX.

and neutron excitations from the $d_{3/2}$ and $s_{1/2}$ shells below the 20 gap to the $f_{7/2}$ shell just above the gap (see Fig. 6). Going towards Ca$_{28}$ the neutron excitations become suppressed as the Fermi level reaches the middle of the $N_{osc} = 3$ shell and proton excitations start to dominate. When more neutrons are added, neutron excitations to the $g_{9/2}$ shell start to appear and become the largest components in Ca$_{40}$.

V. SUMMARY AND CONCLUSIONS

An iterative method for the solution of the QRPA equations which avoids the construction of the large QRPA matrix was employed for the calculation of low-lying vibrational states. The method uses the implicitly restarted Arnoldi approach for the solution of the non-Hermitian eigenvalue problem. In this approach, only the action of the matrix on a Ritz vector is needed. As demonstrated, this can be expressed in terms of the fields generated by the transitional densities corresponding to the Ritz vector. Our study shows that the method is numerically stable and typically requires a few thousand iterations in order to produce well converged lowest eigenstates.

The new solution method was applied to the calculation of excitation energies and decay rates of the first 2^+ and 3^- vibrational states in a set of spherical even-even nuclei. The calculations were performed using three different Skyrme interactions together with a finite-range pairing force. Overall a quite reasonable agreement with experimental data was obtained. The main difficulties seem to be in the description of 2^+ states right between two magic neutron numbers where the different interactions tend to give different results and even zero-energy solutions.

Difficulties were also observed for the Ca isotopes where all the interactions gave too little collectivity. These difficulties are probably related to the limitations of the QRPA method itself, as it only includes two-quasiparticle excitations. However, since our method is rather computationally inexpensive, it may become practical to consider extensions of QRPA, for example higher-order QRPA approaches or boson expansion methods, which allow one to treat more complicated excitations that could improve the results.

Because of the low numerical cost and low memory requirements, the method appears promising for applications to deformed nuclei where the dimensions become substantially larger. Indeed, the methods of this work are quite analogous to the ones used in the nuclear shell model community, where quite similar iterative methods have been used for large-dimensional Hermitian eigenvalue problems. However, contrary to the shell model where the dimensions increase exponentially and multiple major shell calculations for heavy nuclei are almost impossible, the QRPA method stays tractable. Therefore, as a next step, we will implement the method in a code able to treat nuclei with deformed ground states.

For spherical nuclei, the speed of the iterative method opens the possibility to directly compute low-lying states and include them as part of the observables used when fitting the parameters of new improved Skyrme interactions. However, care must be taken to analyze the structure of the included states in order to ensure that a QRPA description is compatible with the experimental states.

[1] P. Ring and P. Shuck, *The Nuclear Many-Body Problem*, 1st ed. (Springer-Verlag, New York, 1980).

[2] T. Nakatsukasa, T. Inakura, and K. Yabana, Phys. Rev. C **76**, 024318 (2007).

[3] P. Avogadro and T. Nakatsukasa, Phys. Rev. C **84**, 014314 (2011).

[4] J. Toivanen, B. G. Carlsson, J. Dobaczewski, K. Mizuyama, R. R. Rodriguez-Guzman, P. Toivanen, and P. Vesely, Phys. Rev. C **81**, 034312 (2010).

[5] V. O. Nesterenko, J. Kvasil, and P.-G. Reinhard, Phys. Rev. C **66**, 044307 (2002).

[6] D. Rudolph (private communication).

[7] J. Goldstone and K. Gottfried, Nuovo Cimento **13**, 849 (1959).

[8] J. P. Blaizot and D. Gogny, Nucl. Phys. A **284**, 429 (1977).

[9] J. P. Blaizot and G. Ripka, *Quantum Theory of Finite Systems* (MIT Press, Cambridge, MA, 1986).

[10] B. G. Carlsson, J. Dobaczewski, J. Toivanen, and P. Vesely, Comput. Phys. Commun. **181**, 1641 (2010).

[11] C. Losa, A. Pastore, T. Dossing, E. Vigezzi, and R. A. Broglia, Phys. Rev. C **81**, 064307 (2010).

[12] E. Chabanat, P. Bonche, P. Haensel, J. Meyer, and R. Schaeffer, Nucl. Phys. A **635**, 231 (1998); **643**, 441(E) (1998).

[13] J. Dobaczewski and P. Olbratowski, Comput. Phys. Commun. **158**, 158 (2004).

[14] J. Terasaki and J. Engel, Phys. Rev. C **74**, 044301 (2006).

[15] W. E. Arnoldi, Q. Appl. Math. **9**, 17 (1951).

[16] Y. Saad, Linear Algebra Appl. **34**, 269 (1980).

[17] R. B. Lehoucq and D. C. Sorensen, SIAM J. Matrix Anal. Appl. **17**, 789 (1996).

[18] ARPACK, http://www.caam.rice.edu/software/ARPACK/.

[19] Y. Tian, Z. Y. Ma, and P. Ring, Phys. Lett. B **676**, 44 (2009); Phys. Rev. C **79**, 064301 (2009); **80**, 024313 (2009).

[20] T. Duguet, Phys. Rev. C **69**, 054317 (2004).

[21] T. Duguet and T. Lesinski, Eur. Phys. J. Special Topics **156**, 207 (2008).

[22] T. Duguet, T. Lesinski, K. Hebeler, and A. Schwenk, Mod. Phys. Lett. A **25**, 1989 (2010).

[23] P. Vesely, J. Toivanen, B. G. Carlsson, J. Dobaczewski, N. Michel, and A. Pastore (unpublished).

[24] M. V. Stoitsov, J. Dobaczewski, W. Nazarewicz, and P. Ring, Comput. Phys. Commun. **167**, 43 (2005).

[25] J. Dobaczewski, W. Nazarewicz, and T. R. Werner, Phys. Scr., T **56**, 15 (1995).

[26] H. Krivine, J. Treiner, and O. Bohigas, Nucl. Phys. A **336**, 155 (1980).

[27] J. Bartel, P. Quentin, M. Brack, C. Guet, and H. B. Håkansson, Nucl. Phys. A **386**, 79 (1982).

[28] J. Terasaki, in *Bulk Nuclear Properties: 5th ANL/MSU/JINA/INT FRIB Workshop*, edited by P. Danielewicz, AIP Conf. Proc. No. 1128 (AIP, New York, 2009), p. 48.

[29] B. A. Brown, Phys. Rev. C **58**, 220 (1998).

[30] S. Raman, C. W. Nestor Jr., and P. Tikkanen, At. Data Nucl. Data Tables **78**, 1 (2000).

[31] G. D. Dracoulis, G. J. Lane, A. P. Byrne, A. M. Baxter, T. Kibédi, A. O. Macchiavelli, P. Fallon, and R. M. Clark, Phys. Rev. C **67**, 051301(R) (2003).

[32] A. Ansari and P. Ring, Phys. Rev. C **74**, 054313 (2006).

[33] J. Dobaczewski, W. Nazarewicz, T. R. Werner, J. F. Berger, C. R. Chinn, and J. Dechargé, Phys. Rev. C **53**, 2809 (1996).

[34] T. Kibeti and R. H. Spear, At. Data Nucl. Data Tables **80**, 44 (2002).

[35] The ENSDF database, http://www.nndc.bnl.gov/ensdf.